Available online at www.sciencedirect.com
ScienceDirect
Journal of Sound and Vibration 298 (2006) 1129–1149
JOURNAL OF SOUND AND VIBRATION
www.elsevier.com/locate/jsvi

Deformation modes in the finite element absolute nodal coordinate formulation

Hiroyuki Sugiyama[a], Johannes Gerstmayr[b], Ahmed A. Shabana[a,*]

[a]*Department of Mechanical Engineering, University of Illinois at Chicago, 842 West Taylor Street, Chicago, IL 60607, USA*
[b]*Institute for Technical Mechanics, Johannes Kepler University of Linz, Altenbergerstr. 69, 4040 Linz, Austria*

Received 16 February 2005; received in revised form 25 April 2006; accepted 16 June 2006
Available online 28 August 2006

Abstract

The objective of this study is to provide interpretation of the deformation modes in the finite element absolute nodal coordinate formulation using several strain definitions. In this finite element formulation, the nodal coordinates consist of absolute position coordinates and gradients that can be used to define a unique rotation and deformation fields within the element as well as at the nodal points. The results obtained in this study clearly show cross-section deformation modes eliminated when the number of the finite element nodal coordinates is systematically and consistently reduced. Using the procedure discussed in this paper one can obtain a reduced order dynamic model, eliminate position vector gradients that introduce high frequencies to the solution of some problems, achieve the continuity of the remaining gradients at the nodal points, and obtain a formulation that automatically satisfies the principle of work and energy. Furthermore, the resulting dynamic model, unlike large rotation finite element formulations, leads to a unique rotation field, and as a consequence, the obtained formulation does not suffer from the problem of coordinate redundancy that characterizes existing large deformation finite element formulations. In order to accurately define strain components that can have easy physical interpretation, a material coordinate system is introduced to define the material element rotation and deformation. Using the material coordinate system, the Timoshenko–Reissner and Euler–Bernoulli beam models can be systematically obtained as special cases of the absolute nodal coordinate formulation beam models. While a constraint approach is used in this study to eliminate the cross-section deformation modes, it is important to point out as mentioned in this paper that lower-order finite elements, some of which already presented in previous investigations, can be efficiently used in thin and stiff structure applications.

1. Introduction

The absolute nodal coordinate formulation has been used in several analytical and experimental investigations related to large deformation problems [1,2]. In this formulation, only the position field is interpolated in order to define a unique rotation field that can be determined using the position vector gradients [1]. Therefore, in the absolute nodal coordinate formulation, finite rotation parameters are not interpolated and are not used as nodal coordinates. The absolute nodal coordinates consist of the absolute

*Corresponding author. Tel.: +312 996 3600; fax: +312 413 0447.
E-mail address: shabana@uic.edu (A.A. Shabana).

0022-460X/$ - see front matter © 2006 Elsevier Ltd. All rights reserved.
doi:10.1016/j.jsv.2006.06.037

position coordinates and gradients. The gradients, as the result of the Polar Decomposition Theorem [3], can be used to define a unique rotation field within the element as well as at the element boundaries and nodes. By so doing, the problem of coordinate redundancy that characterizes existing large deformation finite element formulations that interpolate finite rotation parameters can be avoided. Information about the rotation of the material points can be obtained using the position vector gradients. If the finite rotation parameters introduced as nodal coordinates are defined in the global coordinate system, no corotational frame is used, and no kinematic constraints are imposed to relate the rotation parameters to the position vector gradients, one then has two independent representations for the finite rotations of the material points. As a consequence, information about the rotation can be obtained using two unrelated sources, leading to the problem of coordinate redundancy. For this reason, the solution obtained using the absolute nodal coordinate formulation does not lead to energy drift or violation of the principle of work and energy as it is the case in many existing methods.

While the absolute nodal coordinate formulation can be and has been successfully used in many large deformation and large rotation applications, numerical problems can be encountered in some applications that include very thin and very stiff structures. These numerical problems are the result of high-frequency oscillations induced by the change in gradients used to describe some of the element cross-section deformation modes. While implicit time integrations [4,5], reduced order integrations and the lower-order elements [6–8] can be used to solve these numerical problems, another approach that can be followed and is adopted in this investigation is to use the strain definitions to obtain conditions that can be used to eliminate the insignificant deformation modes of the element cross-section. To this end, local strain components defined in local frames are first defined and used to shed light on the cross-section deformation modes. Using these strain definitions, different models with different orders can be defined by imposing algebraic conditions that can be used to eliminate some of the element cross-section deformation degrees of freedom. It is shown that some of the existing models such as Timoshenko–Reissner, and Euler–Bernoulli beam models can be systematically obtained from the general description used in the absolute nodal coordinate formulation. Furthermore, the reduction procedure described in this paper ensures the continuity of all the gradients at the nodal points. This in turn guarantees the continuity of the stress and strain components at these points on the centerline. Additionally, the resulting reduced order formulation automatically satisfies the principle of work and energy, as in the case of the absolute nodal coordinate formulation, without the need to take any special measures in the numerical integration. The reduction procedure, however, has several drawbacks that include a non-constant mass matrix, non-zero centrifugal and Coriolis forces and/or the need to solve a system of differential and algebraic equations. Therefore, the method discussed in this paper differs from the methods that employ the absolute nodal coordinate formulation with a smaller number of nodal coordinates and presented in previous investigations [6–8]. The use of the reduced set of element nodal coordinates without following a procedure similar to the one presented in this paper can lead to similar models despite the fact that these models may not provide information about the gradients which are not used in the element formulation.

2. Interpolation of the displacement field

In this investigation, a three-dimensional beam element is used in order to discuss the cross-section deformation modes in the absolute nodal coordinate formulation. The displacement field of a three-dimensional beam element can be interpolated using a polynomial cubic in x and polynomials linear in y and z. The following interpolation is previously used for a three-dimensional beam element in the absolute nodal coordinate formulation [1]:

$$\mathbf{r} = \mathbf{a}_0 + \mathbf{a}_1 x + \mathbf{a}_2 y + \mathbf{a}_3 z + \mathbf{a}_4 xy + \mathbf{a}_5 xz + \mathbf{a}_6 x^2 + \mathbf{a}_7 x^3, \tag{1}$$

where $\mathbf{r}$ is the global position vector, x, y and z are the spatial coordinates defined in the element coordinate system, and $\mathbf{a}_i$ are the 3×1 coefficient vectors of the interpolating polynomial used to determine the global position vector. In general, an infinitesimal material element can have at most 12 modes of displacements; three translations, three rigid body rotations, and six strain components. This is the result which is summarized by the Polar Decomposition Theorem that states that the matrix of position vector gradient can be written as the product of two matrices; the first is an orthogonal matrix that can be expressed in terms of

three independent coordinates while the second is the symmetric stretch matrix that defines six independent strain modes of deformation. Note that the rotation field can be uniquely defined using Eq. (1) since this equation can be used to define the matrix of position vector gradients. The use of independent interpolations for the displacement and rotation fields leads to the coordinate redundancy problem that is inherent in many three-dimensional geometrically exact beam models. This independent interpolation of the displacement and rotation fields is conceptually different from the description used in the absolute nodal coordinate formulation in which only the global displacement field is interpolated, as defined by Eq. (1). The kinematic description used in the absolute nodal coordinate formulation can allow for up to 12 modes of displacement for an infinitesimal material element. To this end, the following vector of nodal coordinates is used:

$$\mathbf{e}^k = \left[(\mathbf{r}^k)^{\mathrm{T}} \quad \left(\frac{\partial \mathbf{r}^k}{\partial x}\right)^{\mathrm{T}} \quad \left(\frac{\partial \mathbf{r}^k}{\partial y}\right)^{\mathrm{T}} \quad \left(\frac{\partial \mathbf{r}^k}{\partial z}\right)^{\mathrm{T}} \right]^{\mathrm{T}}, \tag{2}$$

where $\mathbf{r}^k$ is the global position vector of node k, and $\partial \mathbf{r}^k/\partial x, \partial \mathbf{r}^k/\partial y$ and $\partial \mathbf{r}^k/\partial z$ define the gradients of the global position vector at node k. Using the displacement field given by Eq. (1) and the 12 independent coordinates at each node, the global displacement field of the two-node beam element can be expressed as follows [1]:

$$\mathbf{r} = \mathbf{S}(x, y, z)\mathbf{e}, \tag{3}$$

where $\mathbf{S}(x,y,z)$ is the 3×24 element shape function matrix obtained using the polynomial approximation and the definition of the nodal coordinates given by Eqs. (1) and (2), and $\mathbf{e}$, is the 24×1 vector of nodal coordinates of the two-node beam element. This representation ensures inter-element continuity of the global displacement gradients at the nodal points without making any assumptions on the magnitude of the rotation or deformation within the element. Note that the displacement field of the three-dimensional beam element shown in Fig. 1 can also be written as

$$\mathbf{r} = \mathbf{r}^c + y\mathbf{w}^1 + z\mathbf{w}^2, \tag{4}$$

where $\mathbf{r}^c = \mathbf{S}_{\mathrm{I}}(x)\mathbf{e}$, $\mathbf{w}^1 = \mathbf{S}_{\mathrm{II}}(x)\mathbf{e}$, $\mathbf{w}^2 = \mathbf{S}_{\mathrm{III}}(x)\mathbf{e}$ and the shape function matrices used in these displacement fields are, respectively, defined as follows:

$$\left.\begin{aligned} \mathbf{S}_{\mathrm{I}}(x) &= \begin{bmatrix} s_1\mathbf{I} & s_2\mathbf{I} & \mathbf{0} & \mathbf{0} & s_3\mathbf{I} & s_4\mathbf{I} & \mathbf{0} & \mathbf{0} \end{bmatrix} \\ \mathbf{S}_{\mathrm{II}}(x) &= \begin{bmatrix} \mathbf{0} & \mathbf{0} & \bar{s}_1\mathbf{I} & \mathbf{0} & \mathbf{0} & \mathbf{0} & \bar{s}_2\mathbf{I} & \mathbf{0} \end{bmatrix} \\ \mathbf{S}_{\mathrm{III}}(x) &= \begin{bmatrix} \mathbf{0} & \mathbf{0} & \mathbf{0} & \bar{s}_1\mathbf{I} & \mathbf{0} & \mathbf{0} & \mathbf{0} & \bar{s}_2\mathbf{I} \end{bmatrix} \end{aligned}\right\}, \tag{5}$$

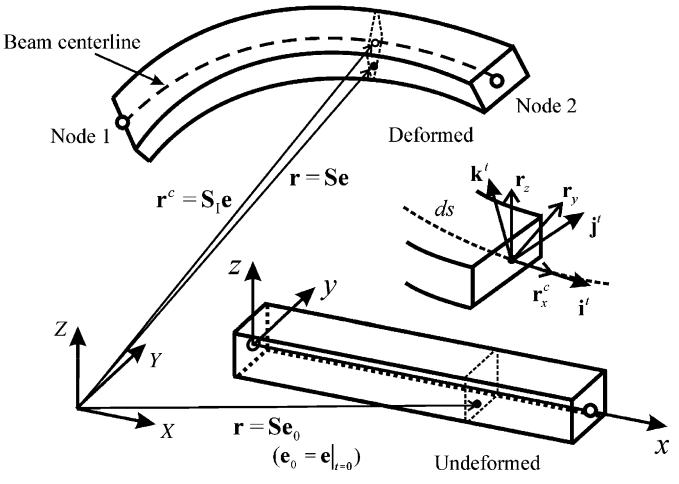

Fig. 1. Absolute nodal coordinates of the beam element.

where

$$\left.\begin{array}{ll} s_1 = 1 - 3\xi^2 + 2\xi^3, & s_2 = \ell(\xi - 2\xi^2 + \xi^3) \\ s_3 = 3\xi^2 - 2\xi^3, & s_4 = \ell(-\xi^2 + \xi^3) \\ \bar{s}_1 = 1 - \xi, & \bar{s}_2 = \xi \end{array}\right\}, \tag{6}$$

and $\xi = x/\ell$ where ℓ is the length of the beam element in the undeformed configuration. It can be seen from the preceding equations that the shape functions are defined by cubic Hermite polynomials that can be used to define the material point position vector along the beam centerline given by $\mathbf{r}^c$ in Eq. (4), while linear polynomials are used for the displacements of the beam cross-section.

Using the displacement field defined by Eqs. (3) or (4), the matrix of the position vector gradients for the beam can be expressed as follows:

$$\mathbf{J} = \partial\mathbf{r}/\partial\mathbf{x}, \tag{7}$$

where $\mathbf{x} = \begin{bmatrix} x & y & z \end{bmatrix}^{\mathrm{T}}$. In the preceding equation, the gradients are obtained using differentiation with respect to the element coordinates x, y, and z. The matrix of gradients in Eq. (7) is related to the matrix of gradients $\mathbf{J}^g$ defined by differentiating the position vector $\mathbf{r}$ with respect to $\mathbf{X} = \mathbf{S}\mathbf{e}_o$ as $\mathbf{J}^g = \mathbf{J}(\partial\mathbf{x}/\partial\mathbf{X})$, where $\mathbf{e}_o$ is the vector of nodal coordinates in the undeformed configuration. Assuming that the beam is initially straight and substituting Eq. (4) into Eq. (7), one has

$$\mathbf{J} = \begin{bmatrix} \mathbf{r}_x^c + y\mathbf{w}_x^1 + z\mathbf{w}_x^2 & \mathbf{w}^1 & \mathbf{w}^2 \end{bmatrix}. \tag{8}$$

In this equation, subscript x indicates differentiation with respect to the element coordinate x; for example, $\mathbf{r}_x^c = \partial\mathbf{r}^c/\partial x$. It is clear from Eq. (8) that $\mathbf{w}^1$ and $\mathbf{w}^2$ define the position vector gradients associated with the spatial coordinates y and z. Therefore, the matrix of the position vector gradients of Eq. (8) can be written as

$$\mathbf{J} = \begin{bmatrix} \mathbf{r}_x^c + y\mathbf{r}_{yx} + z\mathbf{r}_{zx} & \mathbf{r}_y & \mathbf{r}_z \end{bmatrix}, \tag{9}$$

where $\mathbf{r}_y = \partial\mathbf{r}/\partial y$ and $\mathbf{r}_z = \partial\mathbf{r}/\partial z$. It is important to note that, when using a shape function that is linear in y and z, the position vector gradient associated with the element coordinates y and z are defined by the following linear interpolations (see Eqs. (4)–(6)):

$$\left.\begin{array}{l} \mathbf{r}_y = (1 - \xi)\mathbf{r}_y^1 + \xi\mathbf{r}_y^2 \\ \mathbf{r}_z = (1 - \xi)\mathbf{r}_z^1 + \xi\mathbf{r}_z^2 \end{array}\right\}, \tag{10}$$

where $\mathbf{r}_y^k$ and $\mathbf{r}_z^k$ ($k = 1, 2$) represent the gradient nodal coordinates at node k. On the other hand, the gradients associated with the spatial coordinate x are defined by $\mathbf{r}_x^c + y\mathbf{r}_{yx} + z\mathbf{r}_{zx}$. Since the position vector gradients associated with y and z are used to describe the large rigid body motion of the cross-section as well as the deformation, the use of the y and z linear interpolation leads to less accurate definition of strain components as will be discussed in later sections of this paper.

3. Green–Lagrange strains

Using the displacement gradients given by Eq. (9), the Green–Lagrange strain tensor can be obtained as

$$\varepsilon = \frac{1}{2}(\mathbf{J}^{\mathrm{T}}\mathbf{J} - \mathbf{I}), \tag{11}$$

which yields the following nonlinear strain definitions for an initially straight beam:

$$\left.\begin{array}{ll} \varepsilon^{11} = \frac{1}{2}\left(\mathbf{r}_x^c \cdot \mathbf{r}_x^c - 1\right) + y\mathbf{r}_x^c \cdot \mathbf{r}_{yx} + z\mathbf{r}_x^c \cdot \mathbf{r}_{zx} + \varepsilon^{qx} & \\ \varepsilon^{22} = \frac{1}{2}\left(\mathbf{r}_y \cdot \mathbf{r}_y - 1\right), & \varepsilon^{33} = \frac{1}{2}(\mathbf{r}_z \cdot \mathbf{r}_z - 1) \\ \varepsilon^{12} = \frac{1}{2}\left(\mathbf{r}_x^c \cdot \mathbf{r}_y + z\mathbf{r}_{zx} \cdot \mathbf{r}_y + y\mathbf{r}_{yx} \cdot \mathbf{r}_y\right) & \\ \varepsilon^{13} = \frac{1}{2}\left(\mathbf{r}_x^c \cdot \mathbf{r}_z + z\mathbf{r}_{zx} \cdot \mathbf{r}_z + y\mathbf{r}_{yx} \cdot \mathbf{r}_z\right), & \varepsilon^{23} = \frac{1}{2}\,\mathbf{r}_y \cdot \mathbf{r}_z \end{array}\right\}, \tag{12}$$

where ε^{qx} is higher-order shear strain components associated with the deformation of the cross-section defined by

$$\varepsilon^{qx} = \frac{1}{2}\left((y)^2\mathbf{r}_{yx}\cdot\mathbf{r}_{yx} + (z)^2\mathbf{r}_{zx}\cdot\mathbf{r}_{zx}\right) + yz\mathbf{r}_{yx}\cdot\mathbf{r}_{zx}. \tag{13}$$

Note that the strain associated with pure elongation of a beam is defined by the one-dimensional Green strain

$$\varepsilon^{nx} = \frac{1}{2}\left(\mathbf{r}_x^c\cdot\mathbf{r}_x^c - 1\right), \tag{14}$$

where superscript n is used for the normal strain. Similarly, the normal strains produced by pure stretches of the cross-section planes along the y and z directions can be, respectively, expressed as

$$\varepsilon^{ny} = \frac{1}{2}\left(\mathbf{r}_y\cdot\mathbf{r}_y - 1\right), \quad \varepsilon^{nz} = \frac{1}{2}(\mathbf{r}_z\cdot\mathbf{r}_z - 1). \tag{15}$$

Shear strains due to the displacement of the beam cross-section are given by

$$\varepsilon^{sxy} = \frac{1}{2}\,\mathbf{r}_x^c\cdot\mathbf{r}_y, \quad \varepsilon^{sxz} = \frac{1}{2}\,\mathbf{r}_x^c\cdot\mathbf{r}_z, \tag{16}$$

where superscript s refers to shear strains. Similarly, the shear strain in y and z plane is defined by

$$\varepsilon^{syz} = \frac{1}{2}\,\mathbf{r}_y\cdot\mathbf{r}_z. \tag{17}$$

The remaining strain components are functions of deformation modes associated with bending, torsion, and twist of the cross-section. However, since the displacement gradients defined by Eq. (9) allow for the deformation of the cross-section, these strain definitions contain terms that include couplings between the bending/torsion strain components and the deformation of the cross-section as can be seen from Eq. (12). For this reason, more detailed discussions on the deformation modes associated with the rotation strains will be provided in the following sections after introducing local material frames that can be used to conveniently provide a clear physical interpretation of the modes of deformation of the cross-section.

The displacement field given by Eq. (3) can be used to illustrate the deformation modes obtained using the absolute nodal coordinate formulation as shown in Fig. 2. Fig. 2(a) represents a longitudinal stretch, while the bending modes are shown in Figs. 2(b) and (c). Figs. 2(d) and (e) shows the shear deformations of the cross-section, while Fig. 2(f) shows the torsional deformation. It is important to point out that the rotation strains are coupled with the deformation of the cross-section as shown in Eq. (12).

4. Local material frames and the gradients decomposition

In this section, a local finite element cross-section coordinate system is introduced in order to define local strain components. These strain components can be simplified in order to obtain the strain definitions used in Timoshenko–Reissner and Euler–Bernoulli beam theories used in many geometrically exact beam element models [9–11]. The Polar Decomposition Theorem states that the matrix of position vector gradients can be written as the product of two matrices; an orthogonal matrix that defines the rigid body rotation and a stretch matrix that defines the strains and deformation. The orthogonal matrix that can be expressed in terms of three independent parameters defines a frame in which the gradients and strains can be defined. In this section, we consider two alternate forms that can be easily determined using the position vector gradients. These are the tangent frame and the cross-section frame. It can be shown that the orthogonal matrix associated with the tangent frame is the one that appears in the **QR** decomposition of the matrix of the position vector gradients, where **Q** in this case is the orthogonal matrix that defines the orientation of the tangent frame, and **R** is an upper-triangular matrix.

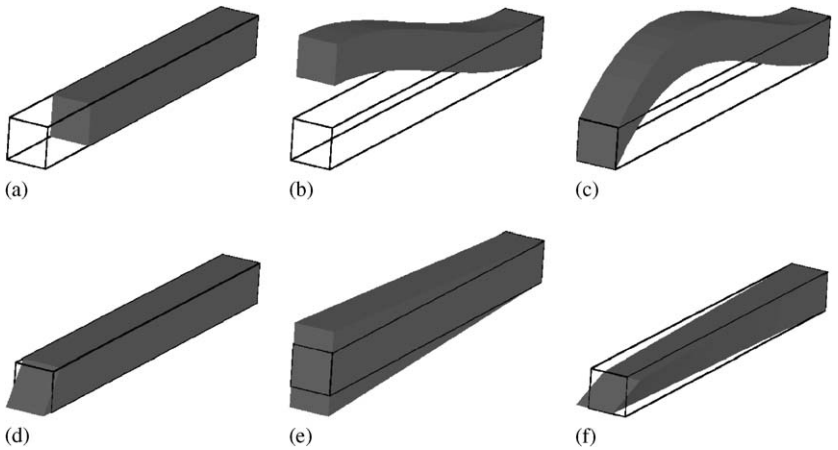

Fig. 2. Deformation modes in the absolute nodal coordinate formulation: (a) longitudinal stretch, (b) bending, (c) bending, (d) shear deformation, (e) stretch of cross-section, (f) torsion.

4.1. Cross-section and tangent frames

A reference frame that can be used for the local definitions of the strains is the cross-section frame. It can be shown that an arbitrary vector defined on the cross-section can be expressed as a linear combination of the two vectors $\mathbf{r}_y$ and $\mathbf{r}_z$. Therefore, using Gram–Schmidt orthogonalization process and the position vector gradients, $\mathbf{r}_y$ and $\mathbf{r}_z$, one can define an orthonormal triad on the deformable beam cross-section as follows [1]:

$$\mathbf{j}^o = \frac{\mathbf{r}_y}{|\mathbf{r}_y|}, \quad \mathbf{k}^o = \frac{\mathbf{r}_z - h\mathbf{r}_y}{|\mathbf{r}_z - h\mathbf{r}_y|}, \quad \mathbf{i}^o = \mathbf{j}^o \times \mathbf{k}^o, \tag{18}$$

where $h = \mathbf{r}_z^{\mathrm{T}}\mathbf{r}_y / \mathbf{r}_y^{\mathrm{T}}\mathbf{r}_y$. Accordingly, the orthonormal orientation matrix can be defined as follows:

$$\mathbf{A}^o = \begin{bmatrix} \mathbf{i}^o & \mathbf{j}^o & \mathbf{k}^o \end{bmatrix}. \tag{19}$$

Another reference frame can be defined using the position vector gradients such that the first axis of the reference frame is always tangent to the beam centerline, $\mathbf{r}_x^c$. Such a coordinate system is called the tangent frame and is defined as follows [12]:

$$\mathbf{A}^t = \begin{bmatrix} \mathbf{i}^t & \mathbf{j}^t & \mathbf{k}^t \end{bmatrix}, \tag{20}$$

where

$$\mathbf{i}^t = \frac{\mathbf{r}_x^c}{|\mathbf{r}_x^c|}, \quad \mathbf{k}^t = \frac{\hat{\mathbf{r}}_x^c \times \hat{\mathbf{r}}_y}{|\hat{\mathbf{r}}_x^c \times \hat{\mathbf{r}}_y|}, \quad \mathbf{j}^t = \mathbf{k}^t \times \mathbf{i}^t, \tag{21}$$

where $\hat{\mathbf{a}}$ denotes a unit vector in the direction of the vector $\mathbf{a}$, that is $\hat{\mathbf{a}} = \mathbf{a}/|\mathbf{a}|$. In the following, the cross-section and tangent frames will be referred to as the *local material frame*.

4.2. Decomposition of displacement gradients

In what follows, it is shown that the use of the tangent frame leads to the definition of the orthogonal matrix that appears in the **QR** decomposition of the matrix of the position vector gradients. That is, the matrix $\mathbf{A}^t$ is the orthogonal matrix $\mathbf{Q}$ that appears in the **QR** decomposition of the matrix of the position vector gradients $\mathbf{J}$ defined on the beam centerline, and $\mathbf{R}$ is an upper-triangular matrix. Using the tangent frame defined by Eqs. (20) and (21), the matrix of the position vector gradients $\mathbf{J}$ can be expressed as follows:

$$\mathbf{J} = \mathbf{A}^t\mathbf{U}^t, \tag{22}$$

where $\mathbf{U}^t = (\mathbf{A}^t)^{\mathrm{T}}\mathbf{J}$. Using the displacement gradients defined by Eq. (9) for the beam element, one can write

$$\mathbf{J} = \mathbf{J}^c + \mathbf{J}^p, \tag{23}$$

where $\mathbf{J}^c$ is the matrix of the position vector gradients defined on the beam centerline, while $\mathbf{J}^p = \mathbf{J} - \mathbf{J}^c$ is a function of the x, y and z coordinates. The matrices $\mathbf{J}^c$ and $\mathbf{J}^p$ can be defined using the displacement field of Eq. (9) as

$$\mathbf{J}^c = \begin{bmatrix}\mathbf{r}_x^c & \mathbf{r}_y & \mathbf{r}_z\end{bmatrix}, \quad \mathbf{J}^p = \begin{bmatrix}\mathbf{r}_x^p & \mathbf{0} & \mathbf{0}\end{bmatrix}, \tag{24}$$

where $\mathbf{r}_x^p(x,y,z) = y\mathbf{r}_{yx} + z\mathbf{r}_{zx}$. Using the decomposition given by Eq. (22), the matrix $\mathbf{U}^t$ can be obtained as

$$\mathbf{U}^t = (\mathbf{A}^t)^{\mathrm{T}}\mathbf{J} = \mathbf{U}^{tc} + \mathbf{U}^{tp}, \tag{25}$$

where

$$\left.\begin{aligned}\mathbf{U}^{tc}(x) = (\mathbf{A}^t)^{\mathrm{T}}\mathbf{J}^c &= \begin{bmatrix}\mathbf{i}^t\cdot\mathbf{r}_x^c & \mathbf{i}^t\cdot\mathbf{r}_y & \mathbf{i}^t\cdot\mathbf{r}_z\\ 0 & \mathbf{j}^t\cdot\mathbf{r}_y & \mathbf{j}^t\cdot\mathbf{r}_z\\ 0 & 0 & \mathbf{k}^t\cdot\mathbf{r}_z\end{bmatrix}\\ \mathbf{U}^{tp}(x,y,z) = (\mathbf{A}^t)^{\mathrm{T}}\mathbf{J}^p &= \begin{bmatrix}\mathbf{i}^t\cdot\mathbf{r}_x^p & 0 & 0\\ \mathbf{j}^t\cdot\mathbf{r}_x^p & 0 & 0\\ \mathbf{k}^t\cdot\mathbf{r}_x^p & 0 & 0\end{bmatrix}\end{aligned}\right\}. \tag{26}$$

In the preceding equations, the following identities obtained from the definitions of the tangent frame are used:

$$\left.\begin{aligned}\mathbf{j}^t\cdot\mathbf{r}_x^c &= |\mathbf{r}_x^c|\,\mathbf{i}^t\cdot\left(\mathbf{k}^t\times\mathbf{i}^t\right) = 0\\ \mathbf{k}^t\cdot\mathbf{r}_x^c &= \frac{|\mathbf{r}_x^c|}{|\hat{\mathbf{r}}_x^c\times\hat{\mathbf{r}}_y|}\hat{\mathbf{r}}_x^c\cdot\left(\hat{\mathbf{r}}_x^c\times\hat{\mathbf{r}}_y\right) = 0\\ \mathbf{k}^t\cdot\mathbf{r}_y &= \frac{|\mathbf{r}_y|}{|\hat{\mathbf{r}}_x^c\times\hat{\mathbf{r}}_y|}\hat{\mathbf{r}}_y\cdot\left(\hat{\mathbf{r}}_x^c\times\hat{\mathbf{r}}_y\right) = 0\end{aligned}\right\}. \tag{27}$$

It is clear from Eq. (26) that, on the centerline of the beam, one has the following decomposition for the matrix of the position vector gradients:

$$\mathbf{J}^c = \mathbf{A}^t\mathbf{U}^{tc}, \tag{28}$$

where $\mathbf{U}^{tc}$ is an upper triangular matrix that depends on the strains. Clearly, the decomposition of Eq. (28) is the **QR** decomposition of the matrix of position vector gradients on the beam centerline, with $\mathbf{Q} = \mathbf{A}^t$ and $\mathbf{R} = \mathbf{U}^{tc}$. Note that the use of the decomposition of Eq. (22) leads to the same definition of the Lagrangian strain components. The proof that the use of the tangent frame leads to the **QR** decomposition is presented later in this section.

4.3. Interpretation

Note that the element of the upper-triangular matrix $\mathbf{U}^{tc}$ defines components that can be related to the stretch and shear deformation on the beam centerline, while the elements of the matrix $\mathbf{U}^{tp}$ that is a function of x, y, and z can be related to rotation strain components; mainly, torsion and bending. When first-order approximations are employed, one can have the following strain components projected on the tangent frame:

$$\begin{aligned}\boldsymbol{\varepsilon} &\simeq \frac{1}{2}\left((\mathbf{U}^t)^{\mathrm{T}} + \mathbf{U}^t\right) - \mathbf{I}\\ &= \begin{bmatrix}\mathbf{i}^t\cdot\mathbf{r}_x^c - 1 & \frac{1}{2}\mathbf{i}^t\cdot\mathbf{r}_y & \frac{1}{2}\mathbf{i}^t\cdot\mathbf{r}_z\\ & \mathbf{j}^t\cdot\mathbf{r}_y - 1 & \frac{1}{2}\mathbf{j}^t\cdot\mathbf{r}_z\\ \text{Sym.} & & \mathbf{k}^t\cdot\mathbf{r}_z - 1\end{bmatrix} + \begin{bmatrix}\mathbf{i}^t\cdot\mathbf{r}_x^p & \frac{1}{2}\mathbf{j}^t\cdot\mathbf{r}_x^p & \frac{1}{2}\mathbf{k}^t\cdot\mathbf{r}_x^p\\ & 0 & 0\\ \text{Sym.} & & 0\end{bmatrix}.\end{aligned} \tag{29}$$

It is clear from these linearized expressions that the contribution of the rotations of the cross-section to the longitudinal strain component is given by $\mathbf{i}^t \cdot \mathbf{r}_x^p = y\mathbf{i}^t \cdot \mathbf{r}_{yx} + z\mathbf{i}^t \cdot \mathbf{r}_{zx}$. However, since $\mathbf{r}_y$ and $\mathbf{r}_z$ are defined using a linear polynomial as given by Eq. (10) for the case of the beam element, the derivatives of $\mathbf{r}_y$ and $\mathbf{r}_z$ become constant along the length [13]. This linear interpolation leads to a less accurate definition of the bending strains when strain definitions given by either Eqs. (12) or (29) are used. For this reason, as will be discussed in the following sections, the use of the curvature definitions given by $\bar{\kappa}_2 = -\mathbf{k}^{\mathrm{T}}(\mathrm{d}\mathbf{i}/\mathrm{d}s)$, $\bar{\kappa}_3 = \mathbf{j}^{\mathrm{T}}(\mathrm{d}\mathbf{i}/\mathrm{d}s)$ leads to more accurate definition of the bending since $\mathbf{i}$ is defined by the vector $\mathbf{r}_x^c$ which is approximated using cubic polynomials as shown in Eqs. (4)–(6), where s is the arc-length parameter.

4.4. Proof of the QR decomposition

In order to prove that the use of the tangent frame leads to the **QR** decomposition of the matrix of the position vector gradients when this matrix is defined along the beam centerline, the matrix $\mathbf{J}^c$ is written as follows:

$$\mathbf{J}^c = \mathbf{QR}, \tag{30}$$

where the orthogonal matrix $\mathbf{Q}$ and the upper-triangular matrix $\mathbf{R}$ are, respectively, obtained using the formula of **QR** decomposition given in standard texts as [14]

$$\mathbf{Q} = \begin{bmatrix} \hat{\mathbf{e}}^1 & \hat{\mathbf{e}}^2 & \hat{\mathbf{e}}^3 \end{bmatrix} \quad \text{and} \quad \mathbf{R} = \begin{bmatrix} \hat{\mathbf{e}}^1 \cdot \mathbf{r}_x^c & \hat{\mathbf{e}}^1 \cdot \mathbf{r}_y & \hat{\mathbf{e}}^1 \cdot \mathbf{r}_z \\ 0 & \hat{\mathbf{e}}^2 \cdot \mathbf{r}_y & \hat{\mathbf{e}}^2 \cdot \mathbf{r}_z \\ 0 & 0 & \hat{\mathbf{e}}^3 \cdot \mathbf{r}_z \end{bmatrix} \tag{31}$$

and

$$\hat{\mathbf{e}}^1 = \frac{\mathbf{r}_x^c}{|\mathbf{r}_x^c|}, \quad \hat{\mathbf{e}}^2 = \frac{\mathbf{r}_y - (\mathbf{r}_y \cdot \hat{\mathbf{e}}^1)\hat{\mathbf{e}}^1}{|\mathbf{r}_y - (\mathbf{r}_y \cdot \hat{\mathbf{e}}^1)\hat{\mathbf{e}}^1|}, \quad \hat{\mathbf{e}}^3 = \frac{\mathbf{r}_z - (\mathbf{r}_z \cdot \hat{\mathbf{e}}^1)\hat{\mathbf{e}}^1 - (\mathbf{r}_z \cdot \hat{\mathbf{e}}^2)\hat{\mathbf{e}}^2}{|\mathbf{r}_z - (\mathbf{r}_z \cdot \hat{\mathbf{e}}^1)\hat{\mathbf{e}}^1 - (\mathbf{r}_z \cdot \hat{\mathbf{e}}^2)\hat{\mathbf{e}}^2|}. \tag{32}$$

It can be shown that the matrix $\mathbf{R}$ in Eq. (31) is the same as the matrix $\mathbf{U}^{tc}$ given by Eq. (26) if the orthogonal matrix $\mathbf{Q}$ is assumed to be the same as the matrix $\mathbf{A}^t = \begin{bmatrix} \mathbf{i}^t & \mathbf{j}^t & \mathbf{k}^t \end{bmatrix}$ that defines the orientation of the tangent frame. It is clear from the first equation of Eq. (32) that the vector $\hat{\mathbf{e}}^1$ of the matrix $\mathbf{Q}$ is equal to $\mathbf{i}^t$ defined by Eq. (21), that is, $\hat{\mathbf{e}}^1 = \mathbf{i}^t$. Using the definition of the vector $\hat{\mathbf{e}}^2$, one can show that

$$|\mathbf{r}_y - (\mathbf{r}_y \cdot \hat{\mathbf{e}}^1)\hat{\mathbf{e}}^1| = \sqrt{|\mathbf{r}_y|^2 - (\mathbf{r}_y \cdot \hat{\mathbf{e}}^1)^2} = |\mathbf{r}_y| \sin\ \phi = |\mathbf{r}_y||\hat{\mathbf{r}}_x^c \times \hat{\mathbf{r}}_y|, \tag{33}$$

where ϕ is an angle between the vectors $\mathbf{r}_y$ and $\hat{\mathbf{e}}^1$ which is the same as $\hat{\mathbf{r}}_x^c$. Using the preceding equation, the vector $\hat{\mathbf{e}}^2$ can be written as

$$\hat{\mathbf{e}}^2 = \frac{\mathbf{r}_y - (\mathbf{r}_y \cdot \hat{\mathbf{e}}^1)\hat{\mathbf{e}}^1}{|\mathbf{r}_y||\hat{\mathbf{r}}_x^c \times \hat{\mathbf{r}}_y|} = \frac{(\hat{\mathbf{r}}_x^c \cdot \hat{\mathbf{r}}_x^c)\hat{\mathbf{r}}_y - (\hat{\mathbf{r}}_x^c \cdot \hat{\mathbf{r}}_y)\hat{\mathbf{r}}_x^c}{|\hat{\mathbf{r}}_x^c \times \hat{\mathbf{r}}_y|} = \frac{(\hat{\mathbf{r}}_x^c \times \hat{\mathbf{r}}_y)}{|\hat{\mathbf{r}}_x^c \times \hat{\mathbf{r}}_y|} \times \hat{\mathbf{r}}_x^c = \mathbf{k}_t \times \mathbf{i}_t \equiv \mathbf{j}_t, \tag{34}$$

where $\hat{\mathbf{r}}_y = \mathbf{r}_y/|\mathbf{r}_y|$ and the identity of the vector triple product is used. As a result, the third vector $\hat{\mathbf{e}}^3$ is equal to $\mathbf{k}_t$ since the orthogonality condition needs to be satisfied for the matrix $\mathbf{Q}$; that is

$$\hat{\mathbf{e}}^3 = \hat{\mathbf{e}}^1 \times \hat{\mathbf{e}}^2 = \mathbf{i}^t \times \mathbf{j}^t \equiv \mathbf{k}^t. \tag{35}$$

This shows that the decomposition of the matrix of the position vector gradients defined on the centerline of the beam leads to the **QR** decomposition if $\mathbf{Q}$ is assumed to be $\mathbf{A}^t$. It is important to point out again that regardless of the factorization used for $\mathbf{J}$, the Green–Lagrangian strain components obtained by $\varepsilon = \frac{1}{2}(\mathbf{J}^{\mathrm{T}}\mathbf{J} - \mathbf{I})$ remain the same, while the first-order approximation of the strains leads to different definitions depending on the choice of the local material frames.

5. Curvature, torsion, and local strain definitions

In this section, the nonlinear strain components of the element cross-section are expressed using the local material frames in order to identify the rotation strain components and their coupling with the deformation of the cross-section. To this end, the gradients at the material point are projected on the material frames and simplifying assumptions regarding the deformation of the cross-section are made in order to provide the interpretation of the nonlinear strain components obtained using the absolute nodal coordinate formulation.

5.1. Curvature and torsion

The orientation of the Serret–Frenet frame associated with the spatial curve representing the beam centerline can be defined using the unit tangent $\mathbf{t}$, normal $\mathbf{n}$, and binormal $\mathbf{b}$. The orientation of this frame can then be defined by the transformation matrix [14]

$$\mathbf{A}^f = \begin{bmatrix} \mathbf{t} & \mathbf{n} & \mathbf{b} \end{bmatrix}. \tag{36}$$

From the theory of curves in differential geometry, one has the following expressions for the derivatives of $\mathbf{t}$, $\mathbf{n}$ and $\mathbf{b}$ [14]

$$\mathbf{t}_s = \bar{\kappa}\mathbf{n}, \quad \mathbf{n}_s = -\bar{\kappa}\mathbf{t} + \bar{\tau}\mathbf{b}, \quad \mathbf{b}_s = -\bar{\tau}\mathbf{n}, \tag{37}$$

where subscript s refers to differentiation with respect to the arc-length s, $\bar{\kappa}$ is the curvature and $\bar{\tau}$ is the torsion. Using the preceding two equations, one can show that

$$\tilde{\bar{\boldsymbol{\kappa}}} = (\mathbf{A}^f)^{\mathrm{T}}\mathbf{A}^f_s, \tag{38}$$

where $\tilde{\bar{\boldsymbol{\kappa}}}$ is the skew-symmetric matrix

$$\tilde{\bar{\boldsymbol{\kappa}}} = \begin{bmatrix} 0 & -\bar{\kappa} & 0 \\ \bar{\kappa} & 0 & -\bar{\tau} \\ 0 & \bar{\tau} & 0 \end{bmatrix}. \tag{39}$$

It can be seen from the preceding equation that torsion is defined as rotation about the tangent $\mathbf{t}$, while curvature is defined as rotation about the binormal $\mathbf{b}$. Note that in the case of the cross-section frame introduced previously in this paper, the first axis can be different from the tangent to the centerline due to the shear deformation. Note that in the case of the tangent frame, the first axis is taken along the tangent. Let

$$\mathbf{A} = \begin{bmatrix} \mathbf{t} & \mathbf{j} & \mathbf{k} \end{bmatrix}, \tag{40}$$

be the transformation matrix that defines the orientation of the material frame.

Recall that

$$\mathrm{d}s = \left|\mathbf{r}^c_x\right| \mathrm{d}x. \tag{41}$$

It follows that

$$\mathbf{A}_s = \frac{1}{\left|\mathbf{r}^c_x\right|}\mathbf{A}_x, \tag{42}$$

where $\mathbf{A}_s = \mathrm{d}\mathbf{A}/\mathrm{d}s$ and $\mathbf{A}_x = \mathrm{d}\mathbf{A}/\mathrm{d}x$.

In the case of the tangent frame, one can write the transformation matrix $\mathbf{A}^t$ that defines the orientation of the tangent frame in the global coordinate system in terms of the matrix $\mathbf{A}^f$ that defines the orientation of the Serret–Frenet frame as follows:

$$\mathbf{A}^t = \mathbf{A}^f\mathbf{A}^{tf}, \tag{43}$$

where $\mathbf{A}^{tf}$ is the matrix that defines the orientation of the tangent frame with respect to the Serret–Frenet frame. This matrix can be expressed in terms of one angle β as follows:

$$\mathbf{A}^{tf} = \begin{bmatrix} 1 & 0 & 0 \\ 0 & \cos\beta & -\sin\beta \\ 0 & \sin\beta & \cos\beta \end{bmatrix}. \tag{44}$$

It follows that

$$(\mathbf{A}^{t})^{\mathrm{T}}\mathbf{A}^{t}_{s} = (\mathbf{A}^{tf})^{\mathrm{T}}\tilde{\bar{\boldsymbol{\kappa}}}\,\mathbf{A}^{tf}, \tag{45}$$

where $\mathbf{A}^{t}_{s} = \mathrm{d}\mathbf{A}^{t}/\mathrm{d}s$. Carrying out the matrix multiplication in Eq. (45), one obtains

$$\tilde{\bar{\boldsymbol{\kappa}}}^{t} = (\mathbf{A}^{t})^{\mathrm{T}}\mathbf{A}^{t}_{s} = \begin{bmatrix} 0 & -\bar{\kappa}\cos\beta & \bar{\kappa}\sin\beta \\ \bar{\kappa}\cos\beta & 0 & -\bar{\tau} \\ -\bar{\kappa}\sin\beta & \bar{\tau} & 0 \end{bmatrix}, \tag{46}$$

where $\tilde{\bar{\boldsymbol{\kappa}}}^{t}$ is the *curvature–torsion matrix* associated with the tangent frame. Using an angle between the binormal $\mathbf{b}$ and the second axis of the tangent frame $\mathbf{j}^{t}$ given by $\gamma = \beta - \pi/2$, the curvature–torsion matrix are written as follows:

$$\tilde{\bar{\boldsymbol{\kappa}}}^{t} = \begin{bmatrix} 0 & -\bar{\kappa}\cos\beta & \bar{\kappa}\cos\gamma \\ \bar{\kappa}\cos\beta & 0 & -\bar{\tau} \\ -\bar{\kappa}\cos\gamma & \bar{\tau} & 0 \end{bmatrix} = \begin{bmatrix} 0 & -\bar{\kappa}\mathbf{b}\cdot\mathbf{k}^{t} & \bar{\kappa}\mathbf{b}\cdot\mathbf{j}^{t} \\ \bar{\kappa}\mathbf{b}\cdot\mathbf{k}^{t} & 0 & -\bar{\tau} \\ -\bar{\kappa}\mathbf{b}\cdot\mathbf{j}^{t} & \bar{\tau} & 0 \end{bmatrix}, \tag{47}$$

which shows that when the tangent frame is used, the rotational component associated with the longitudinal axis remains the same as the torsion defined in Serret–Frenet frame, while the curvature defined about the binormal $\mathbf{b}$ is projected into two axes $\mathbf{j}^{t}$ and $\mathbf{k}^{t}$ that differ from the normal and binormal used in the Serret–Frenet frame.

In general, for any local material frame, by the virtue of the orthogonality of the transformation matrix $\mathbf{A} = \begin{bmatrix} \mathbf{i} & \mathbf{j} & \mathbf{k} \end{bmatrix}$ that defines the orientation of this frame ($\mathbf{A}^{\mathrm{T}}\mathbf{A} = \mathbf{I}$), one always has [9]

$$\tilde{\bar{\boldsymbol{\kappa}}} = \mathbf{A}^{\mathrm{T}}\mathbf{A}_{s}, \tag{48}$$

where $\tilde{\bar{\boldsymbol{\kappa}}}$ is a skew-symmetric matrix associated with the vector $\bar{\boldsymbol{\kappa}} = [\,\bar{\kappa}^{1} \quad \bar{\kappa}^{2} \quad \bar{\kappa}^{3}\,]^{\mathrm{T}}$ where

$$\bar{\kappa}_{1} = \mathbf{k}\cdot\mathbf{j}_{s}, \quad \bar{\kappa}_{2} = -\mathbf{k}\cdot\mathbf{i}_{s}, \quad \bar{\kappa}_{3} = \mathbf{j}\cdot\mathbf{i}_{s}. \tag{49}$$

In this equation, subscript s indicates differentiation with respect to the arc-length parameter s. Note that the definition of the torsion and curvatures associated with the tangent and cross-section frames are different. Using the assumption that the longitudinal axis of the cross-section frame does not significantly differ from the tangent to the beam centerline, $\bar{\kappa}_{1}$ in the preceding equation can be assumed to represent the torsion. One, however, must ensure that the definition of torsion is correctly interpreted when the cross-section frame is used, particularly in the case of large deformation problems.

5.2. Local strain definitions

The position vector gradients along y and z directions of the cross-section are projected on a local coordinate system attached to the material points as follows:

$$\bar{\mathbf{r}}^{y} = \mathbf{A}^{\mathrm{T}}\mathbf{r}_{y} \quad , \bar{\mathbf{r}}^{z} = \mathbf{A}^{\mathrm{T}}\mathbf{r}_{z}, \tag{50}$$

where the matrix $\mathbf{A}$ can be the transformation matrix that defines the cross-section or the tangent frame. Using the preceding equation, the matrix of position vector gradients of Eq. (9) can be written as

$$\mathbf{J} = \begin{bmatrix} \mathbf{r}^{c}_{x} + \mathbf{A}_{x}\bar{\mathbf{r}}^{p} + \mathbf{A}\bar{\mathbf{r}}^{p}_{x} & \mathbf{A}\bar{\mathbf{r}}^{y} & \mathbf{A}\bar{\mathbf{r}}^{z} \end{bmatrix}, \tag{51}$$

where $\bar{\mathbf{r}}^p$ is the local position vector of an arbitrary point on the beam cross-section defined in the local material reference frame:

$$\bar{\mathbf{r}}^p = y\bar{\mathbf{r}}^y + z\bar{\mathbf{r}}^z. \tag{52}$$

Using chain rule of differentiation, the gradients along the spatial x coordinate in Eq. (51) can be expressed in terms of gradients defined by the differentiation with respect to the arc-length as

$$\mathbf{r}_x = \left(\mathbf{t} + \mathbf{A}_s\bar{\mathbf{r}}^p + \mathbf{A}\bar{\mathbf{r}}^p_s\right)s_x, \tag{53}$$

where $s_x = \mathrm{d}s/\mathrm{d}x$ and $\mathbf{t}$ is the unit tangent to the beam centerline given by $\mathbf{t} = \mathrm{d}\mathbf{r}^c/\mathrm{d}s$. This tangent does not necessarily coincides with the vector $\mathbf{i}$ in the case of the cross-section frame due to the shear deformation. Using Eqs. (51)–(53) and utilizing the identities $\mathbf{A}^{\mathrm{T}}\mathbf{A} = \mathbf{I}$ and $\mathbf{t}^{\mathrm{T}}\mathbf{t} = 1$, Green–Lagrange strain components defined in the local material frame can then be written as follows:

$$\left.\begin{aligned}
&\varepsilon^{11} = \varepsilon^l + \left(\bar{\mathbf{t}}\cdot\tilde{\bar{\boldsymbol{\kappa}}}\,\bar{\mathbf{r}}^p + \bar{\mathbf{t}}\cdot\bar{\mathbf{r}}^p_s\right)(s_x)^2 + \varepsilon^{qx}\\
&\varepsilon^{12} = \tfrac{s_x}{2}\left(\bar{\mathbf{t}}\cdot\bar{\mathbf{r}}^y + z\bar{\mathbf{r}}^y\cdot\tilde{\bar{\boldsymbol{\kappa}}}\,\bar{\mathbf{r}}^z + \bar{\mathbf{r}}^y\cdot\bar{\mathbf{r}}^p_s\right)\\
&\varepsilon^{13} = \tfrac{s_x}{2}\left(\bar{\mathbf{t}}\cdot\bar{\mathbf{r}}^z + y\bar{\mathbf{r}}^z\cdot\tilde{\bar{\boldsymbol{\kappa}}}\,\bar{\mathbf{r}}^y + \bar{\mathbf{r}}^z\cdot\bar{\mathbf{r}}^p_s\right)\\
&\varepsilon^{22} = \tfrac{1}{2}(\bar{\mathbf{r}}^y\cdot\bar{\mathbf{r}}^y - 1),\quad \varepsilon^{33} = \tfrac{1}{2}(\bar{\mathbf{r}}^z\cdot\bar{\mathbf{r}}^z - 1),\quad \varepsilon^{23} = \tfrac{1}{2}\bar{\mathbf{r}}^y\cdot\bar{\mathbf{r}}^z
\end{aligned}\right\}, \tag{54}$$

where $\varepsilon^l = \mathrm{d}s^2 - \mathrm{d}x^2/2\mathrm{d}x^2$ is the nonlinear longitudinal strain, $\tilde{\bar{\boldsymbol{\kappa}}}$ is the curvature–torsion matrix defined by Eq. (48), $\bar{\mathbf{t}} = \mathbf{A}^{\mathrm{T}}\mathbf{t}$ and ε^{qx} contains the higher-order strain components as previously defined in Eq. (13). It is important to note from the strain components defined by Eq. (54) that the deformations of the cross-section due to the change in the gradients along y and z contribute to all the six strain components defined in the element coordinate system. In some applications in which the effect of deformations of the cross-section is small such as in the case of the cable problems, these deformation modes can introduce undesirable high frequency oscillations that lead to numerical difficulties when the system equations of motion are solved.

5.3. Special case

In applications where the effect of deformations of the cross-section is negligible, a special case of the general strain formulation presented in this section can be considered in order to avoid the high frequency oscillations. In the special case discussed in the reminder of this section, the beam cross-section is assumed to remain planar and rigid. In such a case, the local displacement gradient vectors associated with the beam cross-section are always constant and given by

$$\bar{\mathbf{r}}^{y*} = [0\quad 1\quad 0]^{\mathrm{T}},\quad \bar{\mathbf{r}}^{z*} = [0\quad 0\quad 1]^{\mathrm{T}}. \tag{55}$$

Using the preceding equation, it is clear that the orthogonality condition $\bar{\mathbf{r}}^y\cdot\bar{\mathbf{r}}^z = 0$ is also satisfied. As a result, the gradients along the y and z axes can be, respectively, defined by the vectors $\mathbf{j}$ and $\mathbf{k}$ of the local material frame as

$$\mathbf{r}_y = \mathbf{A}\bar{\mathbf{r}}^{y*} = \mathbf{j},\quad \mathbf{r}_z = \mathbf{A}\bar{\mathbf{r}}^{z*} = \mathbf{k}. \tag{56}$$

Using these assumption, the strain components defined by Eq. (54) can then be reduced to the following expressions:

$$\left.\begin{aligned}
&\varepsilon^{11} = \varepsilon^l + (z\bar{\kappa}_2\mathbf{t}\cdot\mathbf{i} - y\bar{\kappa}_3\mathbf{t}\cdot\mathbf{i} + \bar{\kappa}_1\mathbf{t}\cdot(y\mathbf{k} - z\mathbf{j}))(s_x)^2\\
&\varepsilon^{12} = \tfrac{1}{2}\,\mathbf{r}^c_x\cdot\mathbf{j} - \tfrac{s_x}{2}\,z\bar{\kappa}_1,\quad \varepsilon^{13} = \tfrac{1}{2}\,\mathbf{r}^c_x\cdot\mathbf{k} + \tfrac{s_x}{2}\,y\bar{\kappa}_1\\
&\varepsilon^{22} = 0,\quad \varepsilon^{33} = 0,\quad \varepsilon^{23} = 0,
\end{aligned}\right\}, \tag{57}$$

where the fact that $s_x\mathbf{t} = \mathbf{r}^c_x$ is utilized. The first term of ε^{11} defines the nonlinear strain associated with the elongation along the beam centerline, the second and third terms define the contribution of the in-plane and out-of-plane bending to the axial strain, and the fourth and fifth terms define the contribution of the torsion due to the change in the orientation of the cross-section expressed by $\mathbf{t}\cdot\mathbf{j}$ and $\mathbf{t}\cdot\mathbf{k}$. If the cross-section remains

perpendicular to the beam arc-length, these shear effects are identically zero. Furthermore, the shear strain components, ε^{12} and ε^{13}, consist of strains due to the change in the orientation of the cross-section defined by $\frac{1}{2}\mathbf{r}_x^c \cdot \mathbf{j}$ and $\frac{1}{2}\mathbf{r}_x^c \cdot \mathbf{k}$ and the torsional strain $\bar{\kappa}_1$.

6. Comparison with existing beam models

The general strain definitions provided in the preceding section can be used to obtain the simpler models that are used in many investigations by making the appropriate assumptions. In this section, it is shown how the Timoshenko–Reissner and Euler–Bernoulli finite element beam models can be obtained from the more general theory presented in the preceding section. Since the existing beam models assume planar cross-section, Eq. (57) is used as the starting point for the strain definitions developed in this section. It is important, however, to point out that many of the assumptions used in the models presented in this section can be relaxed when general absolute nodal coordinate models are used.

6.1. Timoshenko–Reissner beam model

It can be demonstrated that the strain definitions given by Eq. (57) leads to the Timoshenko–Reissner nonlinear beam model [15] that was first used by Simo and Vu-Quoc for geometrically exact finite element beam models [9–11] when the following simplifying assumptions are made:

1. The longitudinal stretch is assumed to be small such that the first order strain can be used as $\varepsilon^l \simeq \mathbf{i} \cdot \left(\mathbf{r}_x^c - \mathbf{i}\right)$.
2. In addition to Assumption 1, the contribution of the longitudinal stretch to the rotation strains is small such that $\mathrm{d}s \simeq \mathrm{d}x$, that is $s_x = 1$.
3. The contribution of the shear deformation due to the change in the orientation of the cross-section to the bending and torsion is small. As a result, it can be assumed that $\mathbf{t} \cdot \mathbf{i} \simeq 1$, $\mathbf{t} \cdot \mathbf{j} \simeq 0$ and $\mathbf{t} \cdot \mathbf{k} \simeq 0$ in the definition of the longitudinal strain.

Using the preceding assumptions, the nonlinear strains given by Eq. (57) can be simplified, leading to the following strain expressions used in many geometrically exact finite element beam models [9–11]:

$$\left.\begin{aligned} &\varepsilon^{11} = \mathbf{i} \cdot \left(\mathbf{r}_x^c - \mathbf{i}\right) - y\bar{\kappa}_3 + z\bar{\kappa}_2 \\ &\varepsilon^{12} = \tfrac{1}{2}\left(\mathbf{r}_x^c \cdot \mathbf{j} - z\bar{\kappa}_1\right), \quad \varepsilon^{13} = \tfrac{1}{2}\left(\mathbf{r}_x^c \cdot \mathbf{k} + y\bar{\kappa}_1\right) \\ &\varepsilon^{22} = 0, \quad \varepsilon^{33} = 0, \quad \varepsilon^{23} = 0 \end{aligned}\right\}, \tag{58}$$

Note that using Assumption 2 that approximates $\mathrm{d}s$ as $\mathrm{d}s \simeq \mathrm{d}x$ in the terms associated with the rotation strain components, the local curvature-torsion matrix is approximated by $\tilde{\bar{\boldsymbol{\kappa}}} \simeq \mathbf{A}^{\mathrm{T}}\mathbf{A}_x$. It can be shown that the longitudinal and shear strains provided in the literature [9] lead to the strains defined in Eq. (58) since $\boldsymbol{\Gamma} = \mathbf{A}^{\mathrm{T}}\mathbf{r}_x^c - [\,1 \quad 0 \quad 0\,]^{\mathrm{T}} = [\,\mathbf{i} \cdot (\mathbf{r}_x^c - \mathbf{i}) \quad \mathbf{r}_x^c \cdot \mathbf{j} \quad \mathbf{r}_x^c \cdot \mathbf{k}\,]^{\mathrm{T}}$.

As discussed in the introduction of the paper, the rotation matrix $\mathbf{A}$ in the absolute nodal coordinate formulation is defined by the gradients of the global displacement field given by Eq. (19) or (20), while most of existing geometrically exact finite element beam formulations define the orientation of the cross-section using the independent interpolation of the rotation parameters. This interpolation of the rotation field leads to numerical problems such as the energy drift and violation of the principle of work and energy [16].

6.2. Euler–Bernoulli beam

When the assumptions of Euler–Bernoulli beam theory are used, the vector $\mathbf{i}$ is always tangent to the space curve that defines the centerline of the beam. For this reason, the vector tangent to the beam centerline, $\mathbf{r}_x^c$, is perpendicular to the vectors $\mathbf{j}$ and $\mathbf{k}$, leading to the following definitions deduced from the strain components

given by Eq. (58):

$$\left.\begin{aligned} \varepsilon^{11} &= \mathbf{i}\cdot\left(\mathbf{r}_x^c - \mathbf{i}\right) - y\bar{\kappa}_3 + z\bar{\kappa}_2 \\ \varepsilon^{12} &= -\tfrac{1}{2}z\bar{\kappa}_1, \quad \varepsilon^{13} = \tfrac{1}{2}y\bar{\kappa}_1 \\ \varepsilon^{22} &= 0, \quad \varepsilon^{33} = 0, \quad \varepsilon^{23} = 0 \end{aligned}\right\}. \tag{59}$$

In such a case, the shear strain components $\frac{1}{2}\mathbf{r}_x^c\cdot\mathbf{j}$ and $\frac{1}{2}\mathbf{r}_x^c\cdot\mathbf{k}$ are equal to zero in order for $\mathbf{r}_x^c$ to remain normal to the cross-section of the beam, leading to the Euler–Bernoulli strain measure.

7. Reduction of the finite element nodal coordinates

In many existing large deformation finite element formulations, independent interpolations are used for the position vector and the finite orientation parameters. When absolute coordinates are used, such kinematic description does not lead to a unique displacement field, since according to the Polar Decomposition Theorem, the rotation field can be uniquely determined using the gradients of the position vector. This problem of coordinate redundancy can be the source of many numerical difficulties in the simulation of flexible multibody system applications. It is shown in this section, how the number of nodal coordinates used in the absolute nodal coordinate formulation can be consistently reduced by developing a set of algebraic constraint equations that can be used to eliminate some of the modes of deformation of the cross-section of the finite element. The use of this procedure can be effective in eliminating the high frequency oscillations that result from the variations of some gradients components when thin and stiff structures are analyzed. The drawbacks are the need to solve a system of differential and algebraic equations and the generalized mass matrix of the finite element is no longer constant if the dependent coordinates are eliminated. The algebraic constraint equations that will be used in this section to reduce the number of nodal coordinates can be obtained for different existing beam models. It is important to point out at this point that the elimination of the high frequency cross-section deformation modes can be efficiently achieved by developing lower order finite elements based on the absolute nodal coordinate formulation.

7.1. Timoshenko–Reissner beam

Timoshenko–Reissner beam assumptions imply that the beam cross-section remains planar, but the cross-section does not necessarily remain perpendicular to the beam centerline. As a result, the condition given by Eq. (55) is imposed in order to eliminate the strain components associated with the deformation of the cross-section. In such a case, the following conditions can be used:

$$(\mathbf{A}^o)^{\mathrm{T}}\mathbf{r}_y - \bar{\mathbf{r}}^{y*} = \mathbf{0}, \quad (\mathbf{A}^o)^{\mathrm{T}}\mathbf{r}_z - \bar{\mathbf{r}}^{z*} = \mathbf{0}, \tag{60}$$

where the matrix $\mathbf{A}^o$ is the cross-section material frame defined by Eq. (18). Note that the preceding conditions lead to total of six equations, while one can show that the following three conditions are sufficient to satisfy the conditions expressed by Eq. (60):

$$\mathbf{C} = \begin{bmatrix} \mathbf{r}_y\cdot\mathbf{r}_y - 1 \\ \mathbf{r}_z\cdot\mathbf{r}_z - 1 \\ \mathbf{r}_y\cdot\mathbf{r}_z \end{bmatrix} = \mathbf{0}. \tag{61}$$

The preceding three scalar equations guarantee that $\varepsilon^{22} = \varepsilon^{33} = \varepsilon^{23} = 0$ and eliminate the modes of deformation of the cross-section, as discussed in Sections 5 and 6. Recall that the general motion of an infinitesimal volume can be described using twelve independent parameters: three translational parameters; three rotational parameters to describe the reference orientation of the volume; and six parameters that define six strain components. As a consequence, three of the six strain components associated with the deformation of the cross-section can be eliminated using Eq. (61).

7.2. Euler–Bernoulli beam

In the Euler–Bernoulli beam theory, in addition to the assumptions used in Timoshenko–Reissner beam theory, the orientation of the cross-section is assumed to remain perpendicular to the beam centerline. In other words, the unit tangent $\mathbf{t}$ is always perpendicular to both $\mathbf{j}^o$ and $\mathbf{k}^o$ that are used to describe the orientation of the cross-section:

$$\mathbf{t}\cdot\mathbf{j}^o=0,\quad \mathbf{t}\cdot\mathbf{k}^o=0, \tag{62}$$

where $\mathbf{t}=\mathbf{r}_s^c=\hat{\mathbf{r}}_x^c$. Since the gradient vectors $\mathbf{r}_y$ and $\mathbf{r}_z$ are, respectively, equal to $\mathbf{j}^o$ and $\mathbf{k}^o$ under the conditions given by Eq. (60), an Euler–Bernoulli beam element can be obtained in the absolute nodal coordinate formulation using the following two additional conditions imposed on the displacement of a material point within an element:

$$\mathbf{C}=\begin{bmatrix}\mathbf{r}_y\cdot\hat{\mathbf{r}}_x^c\\ \mathbf{r}_z\cdot\hat{\mathbf{r}}_x^c\end{bmatrix}=\mathbf{0}. \tag{63}$$

These equations guarantee that shear strain components at the material point given by Eq. (58) are equals to zero; that is

$$\frac{1}{2}\mathbf{r}_x^c\cdot\mathbf{j}^o=0,\quad \frac{1}{2}\mathbf{r}_x^c\cdot\mathbf{k}^o=0. \tag{64}$$

As a result, the virtual work of the elastic forces can be simply written as

$$\delta W=\int_0^\ell (EA\varepsilon^l\delta\varepsilon^l+GI_{xx}\,\bar{\kappa}^1\delta\bar{\kappa}^1+EI_{yy}\,\bar{\kappa}^2\delta\bar{\kappa}^2+EI_{zz}\,\bar{\kappa}^3\delta\bar{\kappa}^3)\mathrm{d}x, \tag{65}$$

where E is Young's modulus, A is cross-section area, G is the modulus of rigidity, I_{xx} is polar moment of area, and I_{yy} and I_{zz} are second moments of area. The strain components are defined in this case by

$$\varepsilon^l=\frac{1}{2}\left(\mathbf{r}_x^c\cdot\mathbf{r}_x^c-1\right),\quad \bar{\kappa}^1=\frac{1}{2}(\mathbf{k}^o\cdot\mathbf{j}_x-\mathbf{j}^o\cdot\mathbf{k}_x),\quad \bar{\kappa}^2\simeq-\mathbf{k}^o\cdot\mathbf{r}_{xx}^c,\quad \bar{\kappa}^3\simeq\mathbf{j}^o\cdot\mathbf{r}_{xx}^c. \tag{66}$$

Note that if the constraint condition of Eq. (61) is satisfied, $\mathbf{j}^o=\mathbf{r}_y$ and $\mathbf{k}^o=\mathbf{r}_z$, leading to the simpler definition of the elastic forces. Furthermore, in Eq. (65), the integration is performed with respect to the x coordinate only since the cross-section remains planar due to the Euler–Bernoulli beam assumptions.

8. Numerical examples

In this section, numerical examples are presented in order to demonstrate the use of different strain definitions that also lead to the use of different numbers of independent nodal coordinates of the finite element. Since the deformation of the cross-section defined by the variation of the position vector gradients along the y and z coordinates of the cross-section can lead to high-frequency oscillations that do not significantly affect the accuracy of the solution in some applications when the absolute nodal coordinate formulation is used, a thin beam is first considered. In order to demonstrate the effect of the cross-section deformation modes, the constraint formulation is used to impose the Euler–Bernoulli beam assumptions as discussed in Sections 6 and 7. Furthermore, a lower-order beam element based on the absolute nodal coordinate formulation which is a special case of the formulation presented in Ref. [8] is used for the purpose of comparison. In this formulation, only the gradient vector along the centerline is used to describe the longitudinal stretch and the rotation strains, leading to a reduced number of nodal coordinates. However, there is an important limitation in using this element since the effect of pure torsion cannot be correctly taken into account when the element is straight. This is not the case when the independent three gradient vectors along x, y and z are used as discussed in the literature [1]. In the case of the higher-order element, for simplicity, the constraint equations used for Euler–Bernoulli beam assumptions are imposed at the nodal points only. That is, Eqs. (61) and (63) hold only at the nodal points. A similar, but conceptually different procedure is used in the literature [17] for an orthonormality condition of direction cosine coordinates.

The variational equations of motion of the higher order element based on Euler–Bernoulli beam assumptions are given as

$$\delta \mathbf{e}^{\mathrm{T}}(\mathbf{M}\ddot{\mathbf{e}} + \mathbf{C}_{\mathbf{e}}^{\mathrm{T}}\boldsymbol{\lambda} - \mathbf{Q}_k - \mathbf{Q}_e) = 0, \tag{67}$$

where $\mathbf{C_e}$ is the Jacobian matrix of the constraint equations of each element given by Eqs. (61) and (63); $\boldsymbol{\lambda}$ is the vector of Lagrange multipliers associated with the internal constraints; $\mathbf{Q}_k$ is the vector of the generalized element elastic forces; $\mathbf{Q}_e$ is the vector of generalized element external forces; and $\mathbf{M}$ is the mass matrix defined as

$$\mathbf{M} = \int_V \rho \mathbf{S}^{\mathrm{T}}\mathbf{S}\,\mathrm{d}V. \tag{68}$$

In this equation, ρ is the material density of the element and $\mathbf{S}$ is the shape function matrix defined in Eq. (3). Note that the mass matrix $\mathbf{M}$ is constant, and as a consequence, the centrifugal and Coriolis inertia force vectors are identically equal to zero [1]. Eq. (67) leads to a system of differential-algebraic equations. The numerical solution procedure to the differential-algebraic equation encountered in constrained multibody system applications can be found in literature [18].

In the following examples, three different finite element models are used: the first model (Model I) uses the higher-order 24 nodal coordinate element as originally presented in the literature [1]; the second model (Model II) imposes the Euler–Bernoulli beam assumptions to Model I in order to consistently eliminate deformation modes of the cross-section as discussed in this investigation; and the third model (Model III) is a reduced order beam element obtained using six nodal coordinates at each node; three translations and the gradient vector along the x coordinate as presented in the literature [8].

8.1. Large deformation planar cantilever beam

A cantilever beam presented in the literature [19,20] is considered in this example. The length, height and width of the beam are assumed to be 2.4 m, 9 mm and 0.2 m, respectively. Young's modulus is assumed to be $1.0\mathrm{E}+6\,\mathrm{N/m^2}$, while the material density is $2770\,\mathrm{kg/m^3}$. A concentrated vertical force is applied at the free end as follows [19]:

$$F(t) = \begin{cases} \frac{F_0}{2}(1-\cos t) & t<1, \\ F_0 & t\geqslant 1, \end{cases} \tag{69}$$

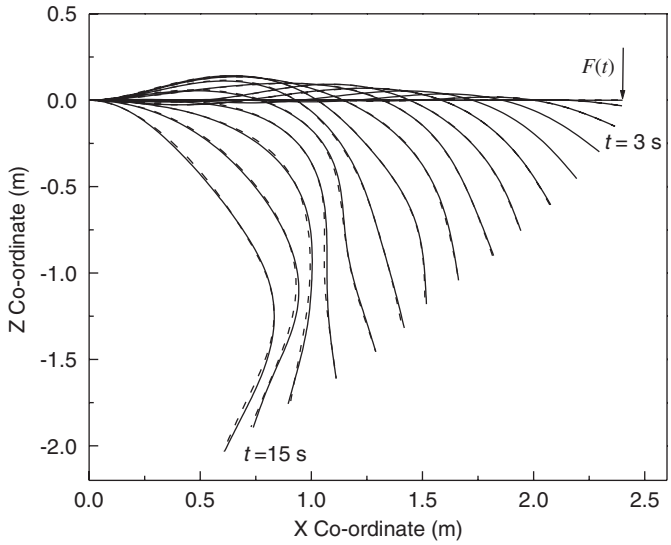

Fig. 3. Deformed shapes of the large deformation cantilever beam problem: —, Model I; --, Model II.

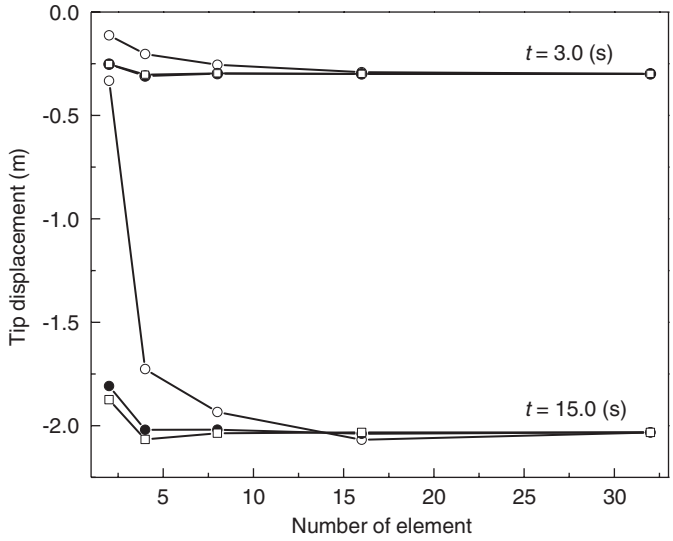

Fig. 4. Effect of the number of elements: -○-, Model I; -●-, Model II; -□-, Model III.

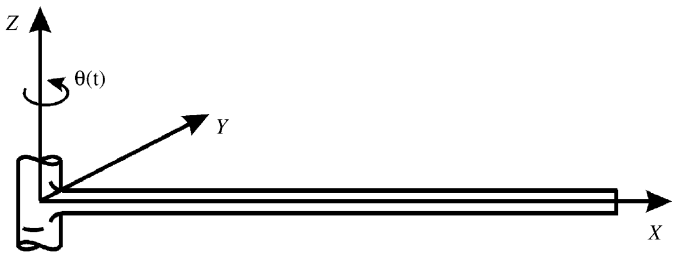

Fig. 5. Spin-up manoeuvre.

where $F_0 = 0.09\,\mathrm{N}$. Fig. 3 shows the deformed shapes of the cantilever beam obtained using 32 elements of Models I and II. In Fig. 4, the vertical tip displacements at time 3 and 15 s are presented for different number of finite elements used. The results presented in this figure show that all the models lead to the convergent solution as the number of elements increases. However, for this thin beam problem, the rate of convergence in the case of Models II and III is better than that of Model I. As discussed in Section 4 for the particular beam element used in this study, the bending strains can be defined in Model I using the derivatives of $\mathbf{r}_y$ and $\mathbf{r}_z$ that are approximated by linear polynomials when Green–Lagrange strains (see Eq. (12)) or the first-order strains (see Eq. (29)) are used. On the other hand, the curvature expression given by Eq. (66) used in Models II and III are defined using the derivatives of $\mathbf{r}^c$ approximated by cubic polynomials. As a result, Models II and III lead to better convergence for the bending strains and their solutions are in good agreement since both models employ the same strain expressions and simplifying assumptions, despite the fact that the two models use different numbers of nodal coordinates and different numerical solution procedures.

8.2. Spin-up maneuver

The spin-up cantilever beam problem shown in Fig. 5 is presented in the second example in order to demonstrate the effect of the geometric stiffening [21,22]. The cross-section is assumed to be rectangular with $A = 7.299\text{E-}5\,\mathrm{m}^2$, and the moment of inertia, the length of the beam, the Young's modulus, and the density are assumed to be $I = 8.215\text{E-}9\,\mathrm{m}^4$, $L = 8\,\mathrm{m}$, $E = 6.895\text{E} + 10\,\mathrm{N/m}^2$, and $\rho = 2766.67\,\mathrm{kg/m}^2$, respectively [22]. The

angular velocity of the hub is prescribed as

$$\theta(t) = \begin{cases} \frac{\omega_s}{T_s}\left(\frac{t^2}{2} + \left(\frac{T_s}{2\pi}\right)^2\left[\cos\left(\frac{2\pi t}{T_s}\right) - 1\right]\right) & 0 \leqslant t \leqslant T_s, \\ \omega_s\left(t - \frac{T_s}{2}\right), & t > T_s, \end{cases} \tag{70}$$

where $T_s = 15$ s and $\omega_s = 4$ rad/s. The simulation is performed for 20 s with a step size of 2 ms. The in-plane tip displacement is measured with respect to a rotating tangential frame rigidly attached to the left-end node that is connected to the rotating hub. Four and eight elements are used in the comparison of different models as shown in Figs. 6 and 7. It can be seen from these figures that all the models properly capture the geometric stiffening effect, while the rate of convergence to the solution in the case of the Models II and III is better than that of Model I as observed in the previous example.

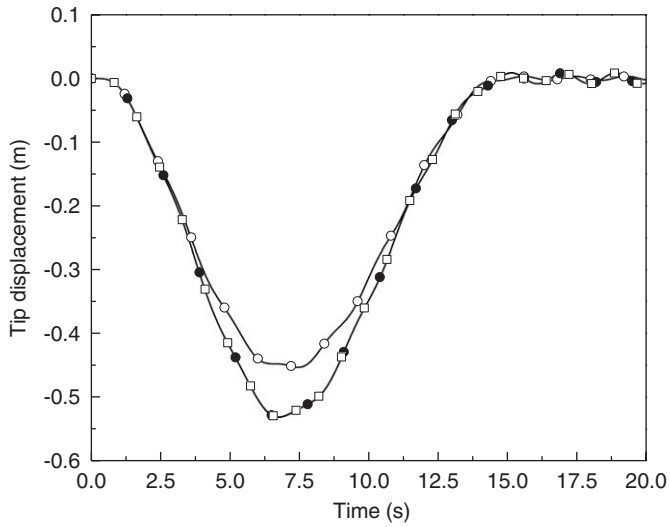

Fig. 6. Tip deformation (four elements): -○-, Model I; -●-, Model II; -□-, Model III.

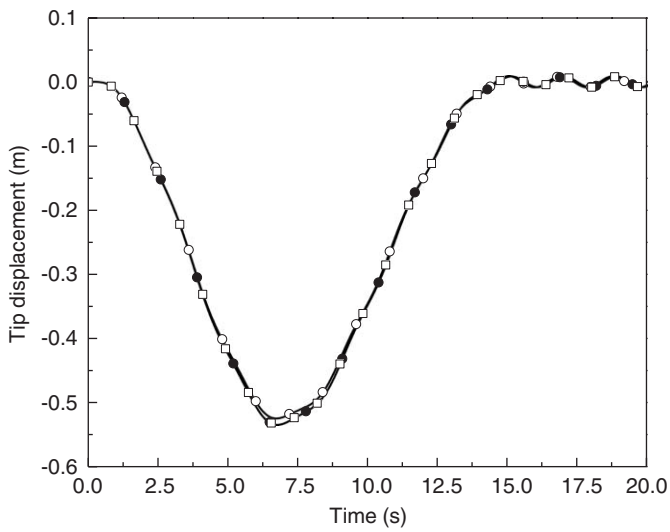

Fig. 7. Tip deformation (eight elements): -○-, Model I; -●-, Model II; -□-, Model III.

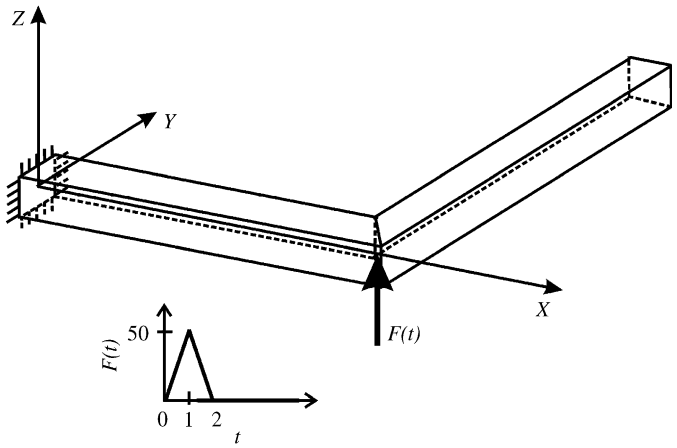

Fig. 8. Right-angle spatial cantilever beam.

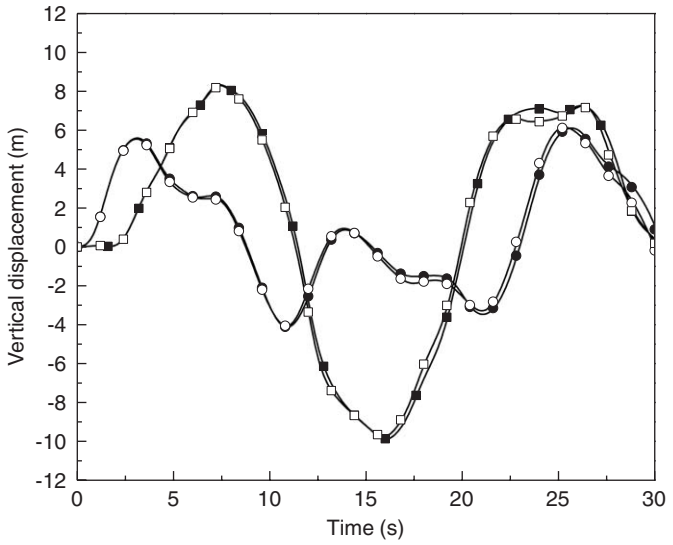

Fig. 9. Veridical displacement: -●-, elbow (four elements); -■-, tip (four elements); -○-, elbow (20 elements); -□-, tip (20 elements).

8.3. Right-angle spatial cantilever beam

A cantilevered L-shaped beam shown in Fig. 8 is used in the third example in order to demonstrate the performance of the formulation for the three-dimensional deformation problem. The example has been first presented by Simo and Vu-Quoc [21] and used by several authors as a benchmark problem [17]. The axial stiffness, the bending rigidity, and the torsional rigidity, are assumed to be $E = 10^6$, $EI = 10^3$, and $GJ = 10^3$, respectively. The mass per unit length is assumed to be $\rho A = 1$, and the mass moment of inertia are assumed to be $\rho I_{xx} = 2\rho I_{yy} = 2\rho I_{zz} = 20$. The cantilever beam is subjected to an out-of-plane concentrated load applied at the elbow and the magnitude of the force is given in Fig. 8. The higher order 24 nodal coordinate element with Euler–Bernoulli assumption (Model II) is used in this example to demonstrate the performance of the formulation. The vertical displacements at the tip and the elbow of the beam are compared for different element discretization: the results obtained using the 4 elements for each arm show good agreement with those of 20 elements as shown in Fig. 9. These results also show good agreement with the results presented in the literature [17,21].

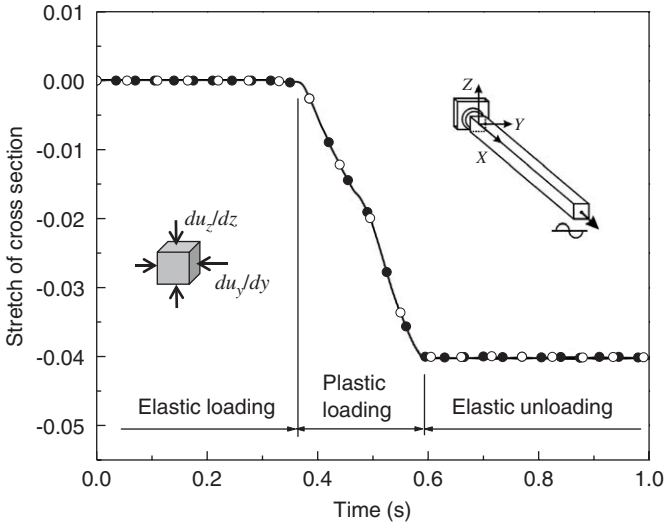

Fig. 10. Deformation of cross-section: -○-, $\partial u_y/\partial y$; -●-, $\partial u_z/\partial z$.

8.4. Cross-section deformation

In the previous examples, the effect of the deformation of the cross-section is assumed to be small for the purpose of comparison. In the following example, the effect of the coupling between the bending and cross-section deformation is presented. As previously shown in Eq. (54), the longitudinal strain component associated with the rotation strains are given by $\varepsilon_r^{11} = \bar{\mathbf{t}} \cdot \tilde{\bar{\boldsymbol{\kappa}}}\, \bar{\mathbf{r}}^p (s_x)^2$. This expression implies that the rotation strain components $\bar{\boldsymbol{\kappa}}$ are coupled with the stretch of the cross-section $\bar{\mathbf{r}}^p = y\bar{\mathbf{r}}^y + z\bar{\mathbf{r}}^z$ defined by the gradient along y and z axes of the element coordinate system. In other words, when the material is subjected to the axial and bending loading simultaneously, the bending stress will be different when the cross-section dimensions change. For example, if the beam is horizontal and subjected to the axial loading, the strain component ε_r^{11} is simplified to the following expression:

$$\begin{aligned}\varepsilon_r^{11} &= \bar{\mathbf{t}} \cdot \tilde{\bar{\boldsymbol{\kappa}}}\, \bar{\mathbf{r}}^p (s_x)^2 \simeq \bar{\mathbf{t}} \cdot \tilde{\bar{\boldsymbol{\kappa}}} (y\bar{\mathbf{r}}^y + z\bar{\mathbf{r}}^z) \\ &= -y\left(1 + \frac{\partial u_y}{\partial y}\right)\bar{\kappa}_3 + z\left(1 + \frac{\partial u_z}{\partial z}\right)\bar{\kappa}_2.\end{aligned}$$

The preceding equation implies that the stretch along the height (z) and width (y) contribute to the change in the bending strains. This can be explained by the fact that the equivalent second moment area changes due to the stretch of the cross-section. This effect can be significant when, for example, elasto-plastic problems are considered since the plastic strains are defined in the deviatoric stress space, leading to the noticeable deformation of the cross-section. Fig. 10 shows the deformation of the cross-section captured by the absolute nodal coordinate formulation for a sinusoidal axial loading scenario presented in literature [23]. In this example, the beam length, the square cross-section area and Young's modulus are assumed to be 1.0 m, 2.5E-3 m^2 and 1.0E + 7 N/m^2, respectively. The external sinusoidal force is assumed to be $F(t) = 300\sin(\pi t)$ N. The initial yield stress and the plastic modulus are assumed to be 1.0E + 5 N/m^2, and 5.0E + 5 N/m^2, respectively. It is demonstrated in this figure that the cross-section shrinks when the material becomes plastic. The coupling between the deformation of cross-section and the bending strains can be observed in the elasto-plastic pendulum problems that involve the large rotational motion of the beam [23]. Fig. 11 shows the total energy that is dissipated by the plastic deformation and the deformation of the cross-section along the height that contributes to the change in the equivalent second moment of area. In this example, the material properties of the flexible pendulum used in this problem are the same as those in the previous problem except for the initial yield stress that is assumed in this example to be equal to 1.2E + 5 N/m^2. It can be seen from these figures that the height of the cross-section is shortened when the plastic loading occurs and the strain associated with

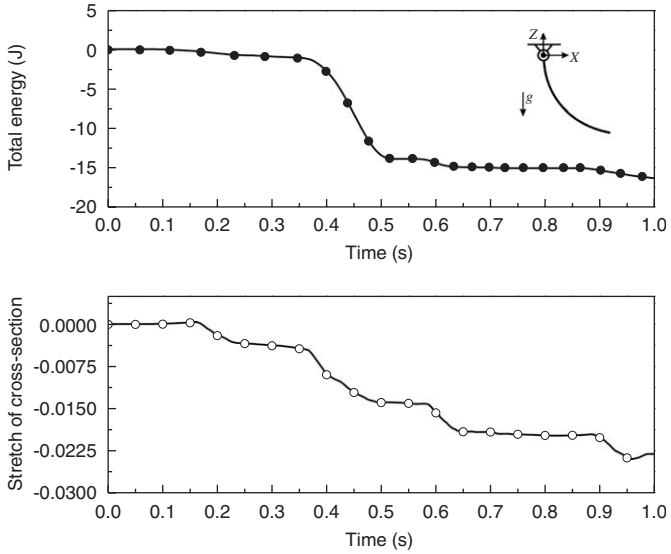

Fig. 11. Elasto-plastic pendulum problem: -●-, total energy; -○-, stretch of cross-section along the height ($\partial u_z/\partial z$).

cross-section is accumulated as the permanent plastic strain. In such a case, the deformation of cross-section cannot be neglected in order to accurately predict the bending motion of the beam that is subjected to the plastic loading.

9. Summary and conclusion

This paper discusses the deformation modes for a three-dimensional beam element obtained using the finite element absolute nodal coordinate formulation. Using the deformation modes discussed in this investigation, a procedure for eliminating modes of deformation of the finite element is presented. Such a procedure leads to a smaller number of independent nodal coordinates and eliminates high frequency oscillations at the expense of having a non-constant coefficient matrix in the acceleration equations, non-zero centrifugal and Coriolis forces and the need to solve a system of differential and algebraic equations. The coordinate reduction procedure presented in this paper requires introducing local frames such as the tangent frame and the cross section frames. The strain components can be defined in these local frames, leading to strain definitions that can be used to obtain, by imposing appropriate assumptions, the simpler models such as the Timoshenko–Reissner and Euler–Bernoulli beam models. The assumptions used to define these models lead to the definition of the algebraic constraint equations that can be used to define a set of dependent coordinates eliminated, thereby reducing the degrees of freedom of the finite element. This coordinate reduction procedure ensures the continuity of the gradients at the nodal points and also leads to the definition of a unique displacement field. Numerical examples are presented in order to demonstrate the use of the beam model obtained using Euler–Bernoulli beam assumptions and these results are compared with those obtained using more general models in the absolute nodal coordinate formulation. Lower-order finite elements based on the absolute nodal coordinate formulation have been also proposed in literature [6–8]. These elements are used in the analysis of thin beam and plate structures without the need for imposing algebraic constraint equations to eliminate high-frequency cross-section modes of deformation.

Acknowledgment

The financial support for the second author by the APART Scholarship of the Austrian Academy of Sciences is gratefully acknowledged.

References

[1] A.A. Shabana, R.Y. Yakoub, Three dimensional absolute nodal coordinate formulation for beam elements, *ASME Journal of Mechanical Design* 123 (2001) 606–621.

[2] W.S. Yoo, J.H. Lee, S.J. Park, J.H. Sohn, O. Dmitrochenko, D. Pogorelov, Large oscillations of a thin cantilever beam: physical experiments and simulation using the absolute nodal coordinate formulation, *Nonlinear Dynamics* 34 (2003) 3–29.

[3] J. Bonet, R.D. Wood, *Nonlinear Continuum Mechanics for Finite Element Analysis*, Cambridge University Press, Cambridge, 1997.

[4] H. Sugiyama, A.A. Shabana, On the use of implicit integration methods and the absolute nodal coordinate formulation in the analysis of elasto-plastic deformation problems, *Nonlinear Dynamics* 37 (2004) 245–270.

[5] D. Garcia-Vallejo, J. Mayo, J.L. Escalona, J. Dominguez, Efficient evaluation of the elastic forces and the Jacobian in the absolute nodal coordinate formulation, *Nonlinear Dynamics* 35 (2004) 313–329.

[6] A.P. Christensen, A.A. Shabana, Exact modeling of the spatial rigid body inertia using the finite element method, *ASME Journal of Vibration and Acoustics* 120 (1998) 650–657.

[7] S. Von Dombrowski, Analysis of large flexible body deformation in multibody systems using absolute coordinates, *Multibody System Dynamics* 8 (2002) 409–432.

[8] O.N. Dmitrochenko, D.Y. Pogorelov, Generalization of plate finite elements for absolute nodal coordinate formulation, *Multibody System Dynamics* 10 (2003) 17–43.

[9] J.C. Simo, L. Vu-Quoc, Three-dimensional finite-strain rod model—Part II: computational aspects, *Computer Methods in Applied Mechanics and Engineering* 58 (1986) 79–116.

[10] A. Cardona, M. Geradin, A beam finite-element non-linear theory with finite rotations, *International Journal for Numerical Methods in Engineering* 26 (1988) 2403–2438.

[11] A. Ibrahimbegovic, On finite element implementation of geometrically nonlinear Reissner's beam theory: three-dimensional curved beam elements, *Computer Methods in Applied Mechanics and Engineering* 122 (1995) 11–26.

[12] H. Sugiyama, J.L. Escalona, A.A. Shabana, Formulation of three-dimensional joint constraints using the absolute nodal coordinates, *Nonlinear Dynamics* 31 (2003) 167–195.

[13] J.T. Sopanen, A.M. Mikkola, Description of elastic forces in absolute nodal coordinate formulation, *Nonlinear Dynamics* 34 (2003) 53–74.

[14] M.D. Greenberg, *Advanced Engineering Mathematics*, Prentice-Hall, Englewood Cliffs, NJ, 1998.

[15] E. Reissner, On finite deformations of space-curved beams, *Journal of Applied Mathematics and Physics (ZAMP)* 32 (1981) 734–744.

[16] G. Jelenic, M.A. Crisfield, Interpolation of rotational variables in nonlinear dynamics of 3D beams, *International Journal for Numerical Methods in Engineering* 43 (1998) 1193–1222.

[17] A. Avello, J. García de Jalón, E. Bayo, Dynamics of flexible multibody systems using Cartesian co-ordinates and large displacement theory, *International Journal for Numerical Methods in Engineering* 32 (1991) 1543–1563.

[18] A.A. Shabana, *Dynamics of Multibody Systems*, third ed., Cambridge University Press, Cambridge, 2005.

[19] R. Iwai, N. Kobayashi, A new flexible multibody beam element based on the absolute nodal coordinate formulation using the global shape function and the analytical mode shape function, *Nonlinear Dynamics* 34 (2003) 207–232.

[20] A.A. Shabana, H.A. Hussien, J.L. Escalona, Application of the absolute nodal coordinate formulation to large rotation and large deformation problems, *ASME Journal of Mechanical Design* 120 (1998) 188–195.

[21] J.C. Simo, L. Vu-Quoc, On the dynamics in space of rods undergoing large motions—a geometrically exact approach, *Computer Methods in Applied Mechanics and Engineering* 66 (1988) 125–161.

[22] S.C. Wu, E.J. Haug, Geometric non-linear substructuring for dynamics of flexible mechanical systems, *International Journal for Numerical Methods in Engineering* 26 (1988) 2211–2226.

[23] H. Sugiyama, A.A. Shabana, Application of plasticity theory and absolute nodal coordinate formulation to flexible multibody system dynamics, *ASME Journal of Mechanical Design* 126 (2004) 478–487.